Molecular Biology of the Cell
Vol. 16, 507–518, February 2005

Slipping or Gripping? Fluorescent Speckle Microscopy in Fish Keratocytes Reveals Two Different Mechanisms for Generating a Retrograde Flow of Actin[V]

Carlos Jurado, John R. Haserick, and Juliet Lee*

Department of Molecular and Cell Biology, University of Connecticut, Storrs, CT 06269

Submitted October 4, 2004; Accepted November 5, 2004
Monitoring Editor: Paul Matsudaira

Fish keratocytes can generate rearward directed traction forces within front portions of the lamellipodium, suggesting that a retrograde flow of actin may also occur here but this was not detected by previous photoactivation experiments. To investigate the relationship between retrograde flow and traction force generation, we have transfected keratocytes with GFP-actin and used fluorescent speckle microscopy, to observe speckle flow. We detected a retrograde flow of actin within the leading lamellipodium that is inversely proportional to both protrusion rate and cell speed. To observe the effect of reducing contractility, we treated transfected cells with ML7, a potent inhibitor of myosin II. Surprisingly, ML7 treatment led to an increase in retrograde flow rate, together with a decrease in protrusion and cell speed, but only in rapidly moving cells. In slower moving cells, retrograde flow decreased, whereas protrusion rate and cell speed increased. These results suggest that there are two mechanisms for producing retrograde flow. One involves slippage between the cytoskeleton and adhesions, that decreases traction force production. The other involves slippage between adhesions and the substratum, which increases traction force production. We conclude that a biphasic relationship exists between retrograde actin flow and adhesiveness in moving keratocytes.

INTRODUCTION

The forward motion of many cell types is accompanied by a retrograde flow of actin filaments within the extending lamella (Grebecki, 1994; Harris, 1994). There has been much interest in this phenomenon because it was thought to reflect the mechanism by which the actin cytoskeleton applies force to the substratum during movement (Harris, 1994; Cramer, 1997). However, the relationship between retrograde flow and traction force generation, is not known.

It is generally accepted that retrograde flow arises from myosin II–dependent contractile forces that pull the cytoskeleton inward with respect to both the substratum and the cell margin (Lin *et al.*, 1996). In addition retrograde flow is dependent on actin polymerization at the leading edge to maintain a continuous supply of F-actin and thus the integrity of the cytoskeleton (Forscher and Smith, 1988). Actin filament polymerization may also contribute to retrograde flow by "pushing" the actin meshwork backward from the leading edge (Fukui *et al.*, 1999; Watanabe and Mitchison, 2002). Evidence for such a mechanism has been found in sea urchin coelomocytes where a retrograde flow that is insensitive to myosin II inhibition occurs at the cell periphery. However, retrograde flow that occurs closer to the cell body, where a high density of myosin II minifilaments is found, decreases after inhibition of myosin II (Henson *et al.*, 1999).

Article published online ahead of print in *MBC in Press* on November 17, 2004 (http://www.molbiolcell.org/cgi/doi/10.1091/mbc.E04-10-0860).

[V] The online version of this article contains supplemental material at *MBC Online* (www.molbiolcell.org).

* Corresponding author. E-mail address: jlee@uconnvm.uconn.edu.

Although retrograde flow is undoubtedly an important aspect of cell movement it can limit the efficiency of protrusion by "subtracting" newly polymerized actin from the leading edge. For example, when the activity of myosin II is inhibited, the rate of retrograde flow decreases, while the rate of protrusion increases (Lin *et al.*, 1996). Consistent with this is the finding that retrograde flow rate is inversely proportional to growth cone advance (Lin and Forscher, 1995) and filopodial elongation (Mallavarapu and Mitchison, 1999). Similarly, retrograde flow is rapid in stationary (Henson *et al.*, 1999) and slow-moving cell types such as nerve growth cones and (Lin *et al.*, 1996), fibroblasts (Wang, 1985) but has not been detected in rapidly moving keratocytes (Theriot and Mitchison, 1991; Lee *et al.*, 1993). The relationship between retrograde flow and protrusion is believed to be determined by a "molecular clutch" that regulates the degree of mechanical coupling between the cytoskeleton and the substratum (Mitchison and Kirschner, 1988; Lin *et al.*, 1994; Suter and Forscher, 1998; Suter and Forscher, 2000). For example, when the clutch is engaged, contractile forces that generate retrograde flow can be transmitted to adhesion receptors, which if immobilized on the substratum, will allow cells to exert traction forces against it. As a result, retrograde flow will decrease while the rate of protrusion increases because actin polymerization will now make a greater contribution to this process. Conversely, if the clutch is disengaged, slippage will occur between the cytoskeleton and adhesion receptors, thus increasing retrograde flow while simultaneously decreasing the rate of protrusion. In addition the decrease in mechanical coupling between the cytoskeleton and the substratum will reduce the amount of force that is transmitted to the substratum.

The molecular clutch is believed to consist of adhesion proteins such as talin, vinculin, and radixin (Jay, 2000) that can form molecular linkages between the β1 subunit of

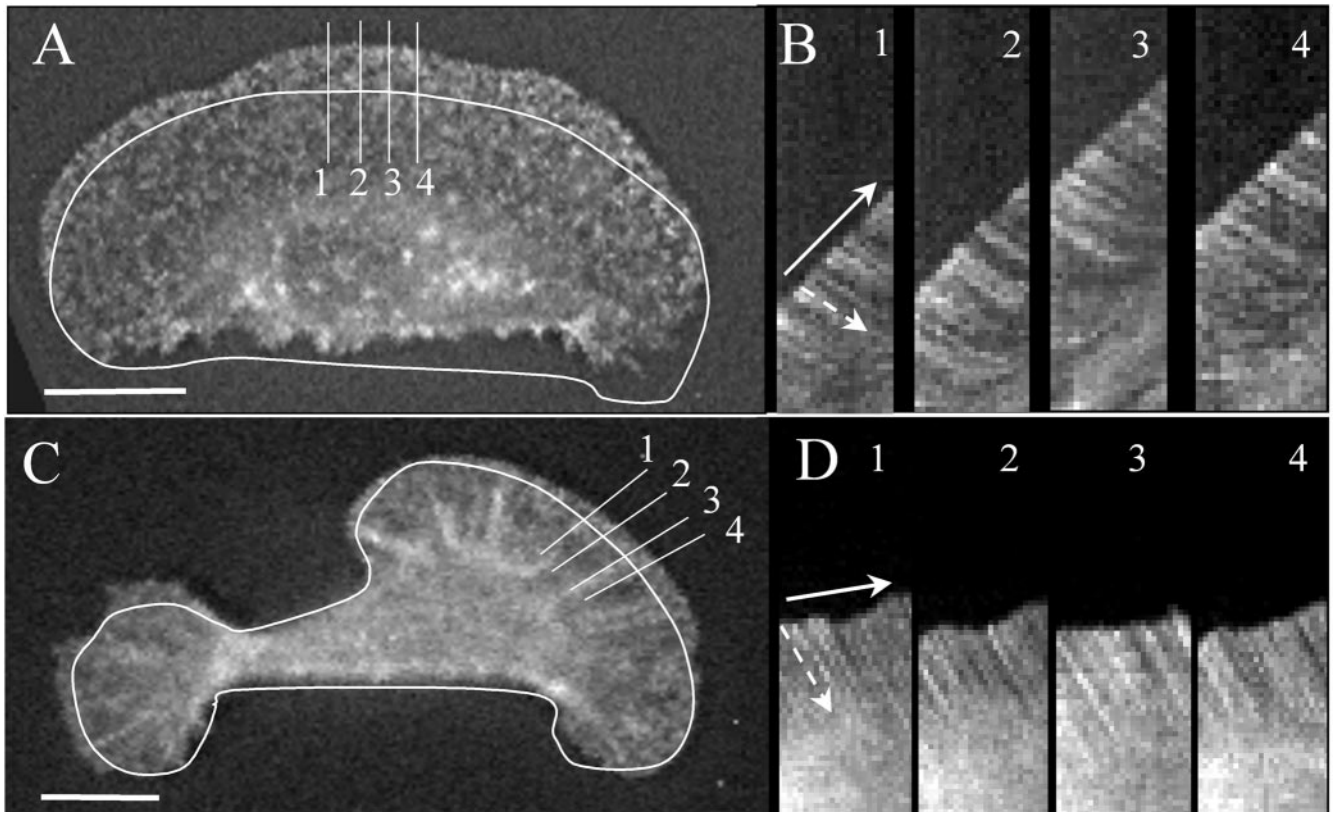

Figure 1. Typical morphology of a fast- (A) and a slow-moving keratocyte (C) displaying fluorescent actin speckles. Outlines represent the position of each cell at the start of the kymographs (B and D) for the cell in A and B, respectively. Each kymograph was obtained from a succession of image "slices" taken from positions indicated by numbered lines, perpendicular to the cell margin and parallel to the direction of movement (bold arrow). The white streaks in each kymograph represent the movement of a single GFP-actin speckle with respect to the substratum. The retrograde flow rate of each speckle was obtained from the slope of its streak (dashed arrows), which is greater in D than B indicating a faster rate of flow in the slow-moving cell (C). Protrusion rate was obtained from the slope created by advance of the cell margin (solid arrow), which is greater in B than D, indicating a more rapid rate of protrusion in the fast-moving cell (A). Bar, 10 μm.

integrins and F-actin. Talin is a particularly strong candidate for a clutch molecule, because it can bind both actin and β1 integrins (Horwitz *et al.*, 1986) and its inactivation in chick DRG neuronal growth cones transiently inhibits filopodial extension and retraction. Because the molecular clutch is essentially an adhesion complex that can transmit contractile forces to the substratum, it will play a pivotal role in regulating the generation of traction force. In fact, it is already well recognized that adhesions influence both the magnitude and spatial pattern of traction force generation (Leader *et al.*, 1983; Lee *et al.*, 1994; Heideman and Buxbaum, 1998; Roy *et al.*, 1999; Balaban *et al.*, 2001; Beningo *et al.*, 2001), which in turn influences the rate and mode of cell movement (Lee *et al.*, 1994; Oliver *et al.*, 1999). In cells that exhibit a slow, discontinuous mode of movement, large traction forces are found facing inward with respect to the front and rear cell margins. However, in keratocytes that display a rapid "gliding" type of movement, the largest traction forces are usually oriented inward at the lateral rear cell margins and perpendicular to the direction of movement. In addition cells that generate the largest traction forces tend to be slow moving and possess numerous focal adhesions (Leader *et al.*, 1983; Munevar *et al.*, 2001) compared with faster moving cell types.

According to the molecular clutch hypothesis, one would expect that regions of high retrograde flow to generate less force on the substratum than regions of slower flow, where the molecular clutch is presumably engaged. However, it is difficult to reconcile this with the fact that in keratocytes, the largest traction forces are seen at the rear lateral edges, where a relatively high retrograde flow was first detected (Theriot and Mitchison, 1991; Lee *et al.*, 1993), whereas much smaller tractions are produced at the leading edge, where retrograde flow was undetectable. In this study, we have transfected fish keratocytes with GFP-actin and used fluorescence speckle microscopy (FSM; Waterman-Storer *et al.*, 1998) to investigate the relationship between retrograde flow, traction force production, in relation to protrusion and rate of cell movement. The major advantage of FSM is that it allows the detection of much slower actin flow rates than either photoactivation or photobleaching techniques. This is because the collective appearance and disappearance of numerous fluorescent actin speckles, provide continuous markers of retrograde flow, over a time scale of minutes, rather than seconds. Keratocytes are particularly well suited for this study because they have a broad, flat lamellipodium that is known to contain a homogeneous meshwork of actin filaments (Svitkina *et al.*, 1997), which facilitates imaging of speckle flow. In addition keratocytes can maintain a relatively constant shape and rate of movement, which is important for the detection of either slow or small changes in retrograde flow rate, because actin filament dynamics is expected to be less variable. Furthermore, the spatial organization of traction forces together with rates of protrusion

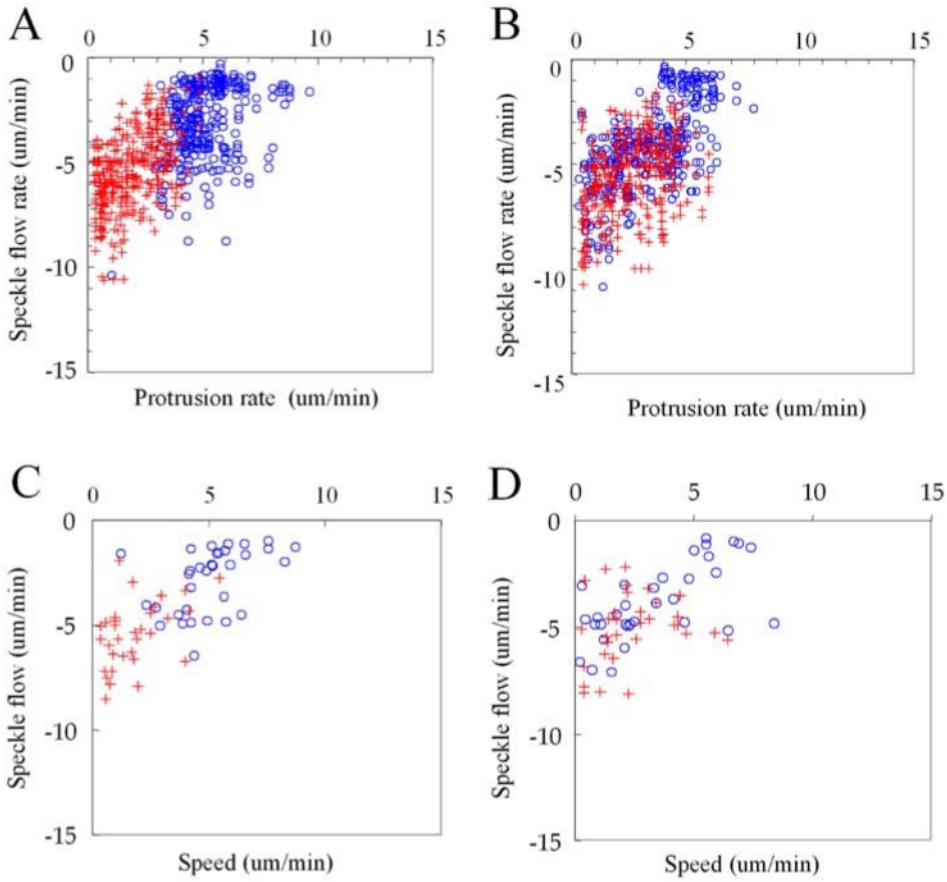

Figure 2. Scatter plots of speckle flow versus protrusion rate before (A) and after (B) treatment with 10 μM ML7. Each data point represents the flow rate of an individual speckle and associated protrusion rate. "Rapid" protrusion rates (>3.5 μm/min) are represented by blue circles, and "slow" (<3.5 μm/min) protrusion rates correspond to red crosses. Comparison of A with B shows a dramatic shift in the distribution of blue, open circles toward toward the lower left of the plot, indicating a decrease in protrusion rate and increase in retrograde speckle flow that follows ML7 treatment. A less marked shift of red crosses toward the upper right represents an increase in protrusion rate and associated decrease in speckle flow rate after treatment. Scatter plot of speckle flow versus cell speed before (C) and after (D) ML7 treatment. A similar shift in the distribution of data points corresponding to fast (>3.5 μm/min, blue, open circles) and slow-moving cells (<3.5 um/min, blue, open circles) occurs as described above.

and retraction will be more stable than in cell types with more complex morphologies.

MATERIALS AND METHODS

Transfection of Fish Keratocytes

Fish epithelial keratocytes were cultured from Molly fish *Poecillia sphenops* scales as described previously (Lee *et al.*, 1993), between a 35-mm glass-bottomed culture dish (Willco-Wells, Amsterdam, The Netherlands) and a coverslip, using L-15 medium supplemented with ~10% fetal bovine serum (FBS). After ~48 h in culture coverslips were removed and cell cultures were washed with phosphate-buffered saline (PBS) containing Ca^{2+} and Mg^{2+}, followed by the addition of 2 ml of culture medium for 2 h. Keratocytes were transiently transfected with the pEGFP-actin construct (CLONTECH, Palo Alto, CA) using the Fugene-6 (Roche Biochemicals, Indianapolis, IN) reagent, according to the manufacturer's protocol, with slight modifications as follows. Before addition of reagent-DNA complexes, culture medium was replaced with 2 ml prewarmed serum-free medium (2 ml). Complex formation between Fugene-6 and plasmid DNA, at a ratio of 3 μl:1 μg per dish, was allowed to form in prewarmed (38°C) serum-free L-15 medium. The reagent-DNA complex solution was added to each well and left for 5 h at room temperature. Next, the complex solution was replaced with 2 ml culture medium supplemented with 200 U/ml penicillin-streptomycin (Life Technologies, Rockville, MD) and 1 μg/ml Fungizone (Life Technologies). The keratocyte cultures were then left overnight to recover and to allow expression of GFP-actin. On average we obtained a transfection efficiency of ~3.5%, with approximately one-third of these cells displaying fluorescent actin speckles, resulting in ~5–20 speckled actin keratocytes per culture dish.

Fluorescent Speckle Microscopy

Before imaging, keratocyte cultures were washed briefly with calcium- and magnesium-free PBS, followed by a second 3-min wash with a 1:1 mixture of PBS and Trypsin-EDTA (Life Technologies) to disaggregate cell sheets, if necessary. Serum-rich (30% FBS) culture medium was added to cells for ~45 min, to quench trypsin activity. Before imaging this was replaced with L-15 medium supplemented with ~2% serum, without antibiotics or antifungal agents, to reduce background fluorescence. Fluorescent actin speckles were imaged on an inverted microscope (Eclipse TE 300; Nikon, Melville, NY) using a Plan APO 100× , 1.4 NA oil immersion objective (Nikon). Fluorescence excitation was achieved using a Ludl high-speed dual filter wheel (Ludl Electronic Products Hawthorne, NY) equipped with a fluorescein excitation filter (490 nm) and 10 or 32% neutral density filters (Chroma Technology, Brattleboro, VT). Fluorescence emission was collected using a FITC filter set (Chroma Technology). Images (16 bit) were acquired using a back-illuminated, back-thinned, frame transfer CCD camera (Quantix 57, Roper Scientific, Tucson, AZ) in 2 × 2 binning mode, using an exposure time of 0.5 s, at intervals ranging between 0.8 and 1.5, and saved on to the computer hard drive. Isee Analytical Imaging Software (Isee Imaging Systems, Raleigh, NC) running on a Unix computer platform (SGI O^2; Silicon Graphics, Mountain View, CA) was used for image acquisition and hardware control.

Interference Reflection Microscopy

To observe changes in the dynamics and types of adhesions formed, the cell-substratum separation distance was imaged using interference reflection microscopy (IRM). This was performed on a Leica DM IRB inverted microscope (Leica, Wetzler, Germany) using a HCX FLUOTAR 100×/0.60–1.30 oil immersion objective. Images were obtained every second using a CoolSnap HQ digital camera (Photometrics, Roper Scientific, Tucson, AZ) controlled by Isee Analytical Imaging Software (Isee Imaging Systems) on a Linux platform. Changes in adhesiveness resulting from ML7 treatment were assessed by generating kymographs, as described below, and then measuring the average gray scale value in a rectangular region, placed just behind the leading edge.

Traction Force Microscopy

Gelatin substrata, whose top surface was embedded with 0.2-μm fluorescent marker beads, were prepared as described previously (Doyle *et al.*, 2002). For each period of observation a series of images is obtained of beads in their displaced positions together with a single reference image of beads in their undisplaced positions, after the cell has moved away. Displacement of the substratum was calculated by comparing the positions of marker beads between the disturbed and reference image, using a correlation based optical flow algorithm (Marganski *et al.*, 2003). Traction maps were generated using the traced cell outline as a guide, and a custom algorithm was then used to

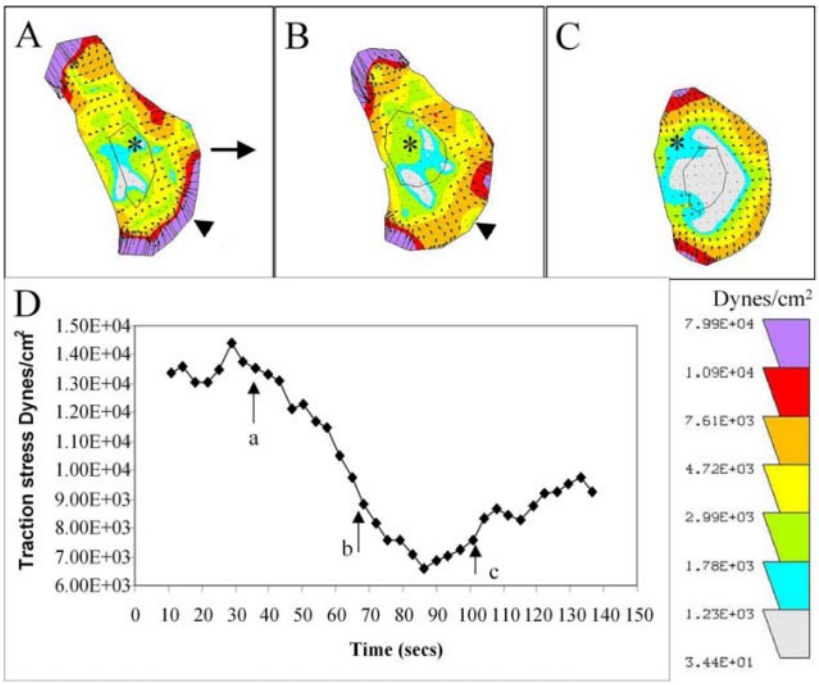

Figure 3. (A–C) Sequence of traction maps showing a decrease in traction force after ML7 treatment. The length and orientation of arrows indicate the magnitude and direction of traction stress exerted on the substratum. Each color represents an area of equal traction stress magnitude. ML7 leads to a rapid decrease in traction stress that is most obvious at the leading edge and lateral right edge (B, arrowhead). Traction stress decreases throughout the cell except at the lateral edges (C). A stationary reference mark (asterisk) has been placed at the center of each panel. (D) Plot of the 90th percentile traction stress over time, with points (a–c) corresponding to A–C indicated (arrows). This shows a ~50% decrease in traction stress occurring within 23 s.

generate a mesh of ~200 quadrilateral elements tessellating the interior of the cell. The most likely traction vector at each node of this mesh is then estimated by fitting the displacement data using the formulas of Boussinesque relating substrate displacement to delta function forces acting at the substrate surface (Dembo and Wang, 1999).

Image Analysis

Morphometric analyses were performed using Metamorph analysis software (Universal Imaging, West Chester, PA). Analysis of actin speckle flow and protrusion rate was performed as described previously (Waterman-Storer *et al.*, 1998). Briefly, the Metamorph line tool, 1 pixel wide, was placed perpendicular to the front cell edge, parallel to flow of speckles (Figure 1, A and B). The kymograph function was used to extract strips at the position of the line, from each sequential image (~30–40), assembling them from left to right, to create a composite image (Figure 1, B and D). The rate of protrusion was calculated from the slope created by the forward advance of the front cell edge. Similarly, the rate of speckle flow was obtained from the slope of white streaks corresponding to the retrograde flow of individual speckles over time. For each observation ~5–8 kymographs were obtained at different locations along the leading edge and ~3 speckles were obtained from each kymograph. The rate of protrusion was taken from the average of all kymographs, and the rate of retrograde speckle flow was obtained from an average of ~20 speckles. The *x,y* coordinates of the cell centroid or of a point at the middle of the back cell edge were used to generate the Rose plots and for calculation of average cell speed. The directionality of cell movement was expressed as a "persistency" factor (Euteneuer and Schliwa, 1984), which is defined as the total distance moved divided by the straight-line distance between the starting and end point of a given time interval.

Myosin II Inhibition

ML-7, an inhibitor of myosin light chain kinase (Saitoh *et al.*, 1987) was made up from a 2 mM stock solution in absolute ethanol. Before use, this was diluted into L-15 medium supplemented with ~2% FBS, to a final working concentration of 10 μM ML7. At this concentration the activity of ML7 is below the inhibitory concentration for other protein kinases (Saitoh *et al.*, 1987). Keratocytes were treated by gently aspirating culture medium from the culture dish, in situ and replacing it with ML7-containing medium. For the collection of paired data sets, a single fluorescent speckled keratocyte was imaged 1–2 min before treatment with ML7 and for ~5 min afterward. Unpaired data sets were collected by imaging a group (2–5) of keratocytes before treatment and a different group afterward.

Immunofluorescence

Immunofluorescence staining was performed as described previously (Doyle and Lee, 2005). Briefly, cells were cooled to 4°C in Fish Ringer's solution before fixation, in 2.5% glutaraldehyde (EMS) and 1:200 fluorescein phalloidin (Molecular Probes, Eugene, OR) for 40 s, followed by 1 min in 1.0% glutaraldehyde and 1:200 fluorescein phalloidin in PBS. Cells were permeabilized in 0.25% Triton X-100 and 1:200 fluorescein phalloidin in PBS for 4 min. After blocking nonspecific binding sites with 1.0% bovine serum albumin for 15 min, cells were labeled with a primary anti-vinculin (mouse) antibody (Sigma, 1:100) in PBS for 30 min and then with the Alexa fluor 568 anti-mouse (Molecular Probes, 1:200) secondary antibody in PBS for 30 min. Coverslips were mounted using Antifade (Molecular Probes).

Shear Flow Experiments

To assess relative changes in cell adhesiveness, after ML7 treatment, shear flow experiments were performed as described previously (Moazzam *et al.*, 1997). Micropipettes with a tip diameter of ~6 μm were made using a Flaming Brown programmable micropipette puller, model P-97 (Sutter Instruments, Novato, CA) and filled with RPMI culture medium supplemented with 1% fetal calf serum. Microneedles were positioned 50–75 μm away from the cell edge, and raised ~25 μm up from the substratum. A jet of medium was produced by using a pressure injector, model MPPI-2 (Applied Scientific Instrumentation, Eugene, OR) to apply pressurized air (between 15 and 24 psi) to the fluid within the micropipette, for a 1-s duration. A rough estimate of the shear force generated in this manner was made by measuring the deflection of a piece of Constantan wire (0.001" diameter, Omega Engineering, Stamford, CT), whose bending modulus was known for a given level of applied air pressure, and distance from the micropipette. This value was divided by the area of the wire impinged on by the jet of fluid. The experiment was performed by first determining the level of shear force required to induce lamellar peeling or deflection of the cell body, in the majority of cells. After addition of ML7 and using the same microneedle and level of air pressure, shear force was applied to single locomoting keratocytes. Videotape recordings of experiments were then used to determine the number and type of cellular response to shear flow.

RESULTS

A Retrograde Flow of Actin Exists within the Front of the Lamellipodium and Is Inversely Related to Rate of Protrusion and Cell Speed

Previous studies of actin filament dynamics failed to detect any retrograde flow of actin within the leading lamellipodium of keratocytes (Theriot and Mitchison, 1991; Theriot and Mitchison, 1992). However, because these studies relied on detecting the movement of a photoactivated mark, slow

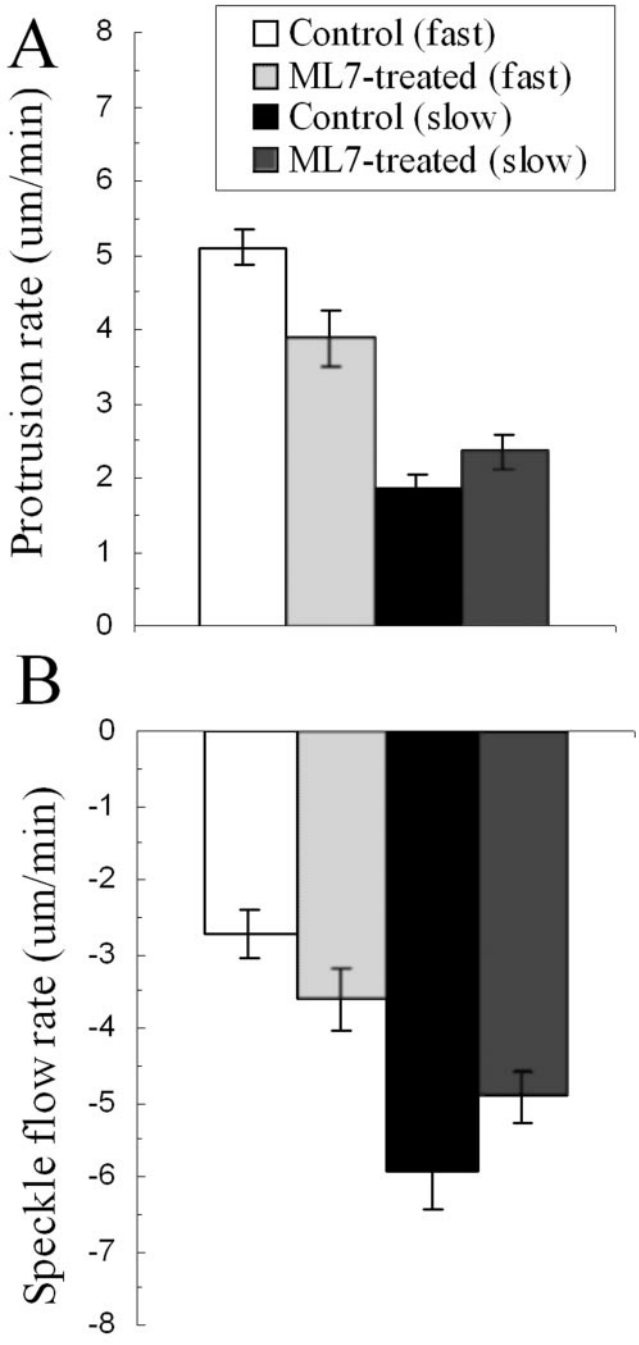

Figure 4. (A) Histogram showing the differential effect of ML7 treatment on the average rates of protrusion in cells with fast compared with slow protrusion rates. (B) Histogram showing the differential effect of ML7 treatment on the average rates of retrograde actin speckle flow in fast- compared with slow-moving cells. Error bars, SE; *Significance, $p \leq 0.05$, $n = 21$.

rates of flow may not have been detectable. We have found that keratocytes can be transfected with GFP-actin and that this results in a small percentage of cells exhibiting fluorescent speckles (Figure 1, A and C; Supplementary Videos GFPspeckle_1 and GFPspeckle_2). In most cells examined actin speckles could be seen flowing inward, both with respect to the cell surface and the substratum, along all sections of the cell margin. Because this was the first time a retrograde flow of actin has been detected within the leading lamellipodium, we examined the relationship between the rates of retrograde flow, protrusion, and cell speed. To do this, we collected image sequences of GFP-actin speckled keratocytes speckles moving over a range of speeds and used kymograph analysis (Figure 1, B and D) to obtain measurements of retrograde speckle flow (with respect to the substratum) and protrusion rates. We found speckle flow rate to be inversely related to the rate of protrusion (Figure 2A). For higher protrusion rates, between 4 and 9 μm/min, retrograde actin flow rates were low, ranging from 0 to 5 um/min. For lower protrusion rates, between 0 and 4 μm/min, retrograde flow rates varied from 2 to 10 μm/min. A similar inverse relationship was found between speckle flow and cell speed (Figure 2C), emphasizing the interrelationship between the regulation of retrograde flow and cell movement. Together these data are consistent with the idea that a molecular clutch mechanism is regulating the degree of mechanical coupling between the cytoskeleton and the substratum. A further implication of these findings is that actin polymerization is constant, whereas the proportion of newly polymerized actin that contributes to protrusion is controlled by the molecular clutch.

Myosin II Inhibition Leads to Opposing Effects in Fast- Versus Slow-moving Keratocytes

According to the molecular clutch hypothesis, retrograde flow is driven primarily by myosin II–dependent contractile forces that cause the cytoskeleton to slip rearward with respect to cell-substratum adhesions (Mitchison and Kirschner, 1988; Lin *et al.*, 1994; Suter and Forscher, 1998). Therefore, inhibition of myosin II in keratocytes is expected to reduce retrograde flow and increase the rates of protrusion, as has been observed previously in *Aplysia* growth cones (Lin *et al.*, 1996). To test this idea we used ML7 to inhibit contractility because it is a potent, highly specific inhibitor of myosin light chain kinase (Saitoh *et al.*, 1987). Using a gelatin traction force assay (Doyle and Lee, 2002), we measured the rate and magnitude of change in traction stress, an indicator of cytoskeletal contractility, resulting from ML7 treatment. We found, on average a significant ~41% decrease in traction stress, within 1–2 min (Figure 3) after treatment in all cells. The average 90th percentile traction stress in pretreated cells was $2.2 \times 10^{+4}$ Dynes/cm^2 ($n = 5$, SEM = $5.9 \times 10^{+3}$ Dynes/cm^2) and dropped to $1.2 \times 10^{+4}$ Dynes/cm^2 ($n = 5$, SEM = $2.6 \times 10^{+3}$ Dynes/cm^2).

Fish keratocytes exhibiting GFP-actin speckles were observed for ~1 min before addition of 10 μM ML7 and then for an additional 1–3 min afterward. The rates of actin speckle flow versus protrusion and cell speed were obtained as described above (Figure 2, B and D). In both treated and untreated keratocytes, retrograde speckle flow is inversely related to protrusion rate. However, after comparing the effects of ML7 treatment on speckle flow in each cell, we noticed that speckle flow was increased or decreased depending in the initial rate of protrusion. To determine the significance of these changes, cells were sorted into groups that had protrusion rates greater or less than 3.5 μm/min, which we termed fast and slow, respectively. This value was chosen because it is the average for all protrusion rates for untreated cells and it represents a break in the frequency distribution of these values (unpublished data). In addition the majority of cells with fast protrusion rates were "fan" shaped, whereas cells with slow protrusion rates were often irregular or fibroblastic in shape (Figure 1C). For cells with fast protrusion rates we found that ML7 treatment led to a

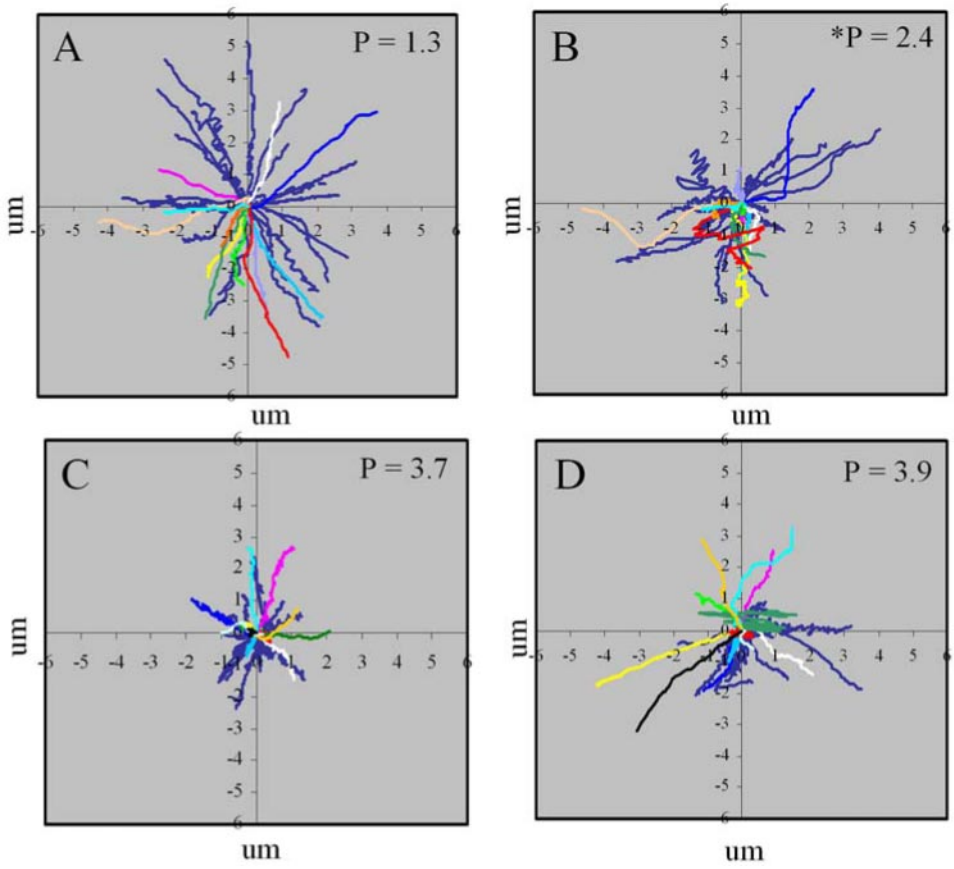

Figure 5. Rose plots showing the opposing effects of ML7 on the directionality of cell movement, between fast- (A and B) and slow- (C and D) moving cells. Blue lines represent unpaired data, colored lines represent paired data, where each color corresponds to a single cell. A decrease in the net cell displacement and directionality occurs in fast-moving cells, after treatment, as indicated by the significant ($p < 0.05$) increase in persistency factor (P). In contrast an increase in net cell displacement and directionality occurs in slow-moving cells after treatment, but the decrease in persistency factor was not significant.

significant decrease in the average protrusion rate, together with a significant increase in retrograde flow (Figure 4; Supplementary Video GFPspeckle_1) for both paired and unpaired data sets (n = 33). Conversely, if the protrusion rate was initially below average, ML7 treatment resulted in an increase in protrusion and a decrease in retrograde flow rate (Figure 4; Supplementary Video GFPspeckle_2), in both data sets but was only significant, for the unpaired data set (n = 20). Together these data suggest that a reduction in contractility leads to disengagement of the molecular clutch, in fast-moving cells and hence decreases the efficiency of protrusion. However, in slow-moving cells reduced contractility leads to engagement of the molecular clutch, thus increasing the efficiency of protrusion.

The inhibition of myosin II also led to opposing effects on speckle flow and cell speed, depending on whether the initial rate of movement was fast (>3.5 μm/min) or slow (<3.5 μm/min, Figure 2, C and D). In fast-moving cells ML7 treatment led to a decrease in speed and increase in retrograde speckle flow, whereas in slow-moving cells, speed increased and flow rate decreased. This differential effect on cell speed was not specific to ML7, we found that 50 μM blebbistatin could produce a similar, though less pronounced effect (unpublished observation). Rose plots of individual cell movement shows that the decrease in speed of fast-moving cells, after ML7 treatment, is accompanied by a reduction in the directionality of cell movement as shown by the significant increase in persistency factor (Figure 5, A and B). Conversely, in slow-moving cells, increased speed tends to be associated with greater directionality that is reflected by the decrease in persistency factor, although this change was not statistically significant.

Inhibition of Myosin II Leads to a Weakening of Cell Substratum Adhesions

Because adhesions have been shown to weaken in response to decreased contractility (Leader *et al.*, 1983; Chrzanowska-Wodnicka and Burridge, 1996; Oliver *et al.*, 1999), it is likely that the differential effects of ML7 on fast- and slow-moving cells might involve changes in adhesiveness. To investigate this possibility, we first used IRM to observe dynamic changes in adhesion sites after ML7 treatment (Figure 6). The various shades of gray in an IRM image result from differences in the separation distance between the ventral cell surface and the substratum and have been shown to correspond to varying degrees of adhesiveness (Paddock, 1989; Davies *et al.*, 1993, 1994). Focal contacts appear as black "streaks" that correspond to a cell-substratum separation distance of ~20–30 nm, whereas the separation distance of close contacts can range between ~30 and 100 nm and appear as diffuse regions of dark gray to white. Fish keratocytes have been shown to possess a broad band of highly dynamic close contacts along the leading edge and can also form small focal adhesions (Lee and Jacobson, 1997). We found that in all cells, irrespective of speed, adhesions at the leading edge appeared to become weaker, as shown by the general enlargement of more distant (white) contacts within a band just behind the leading edge (Figure 6, A and B). To quantitate this change, kymographs were made from pre- and posttreatment image sequences, and the average brightness was measured within a region of close contact behind the leading edge (Figure 6C). We found a significant ~10% (n = 15) increase in the average brightness of close contact at the leading edge over an ~30-s period after treatment (com-

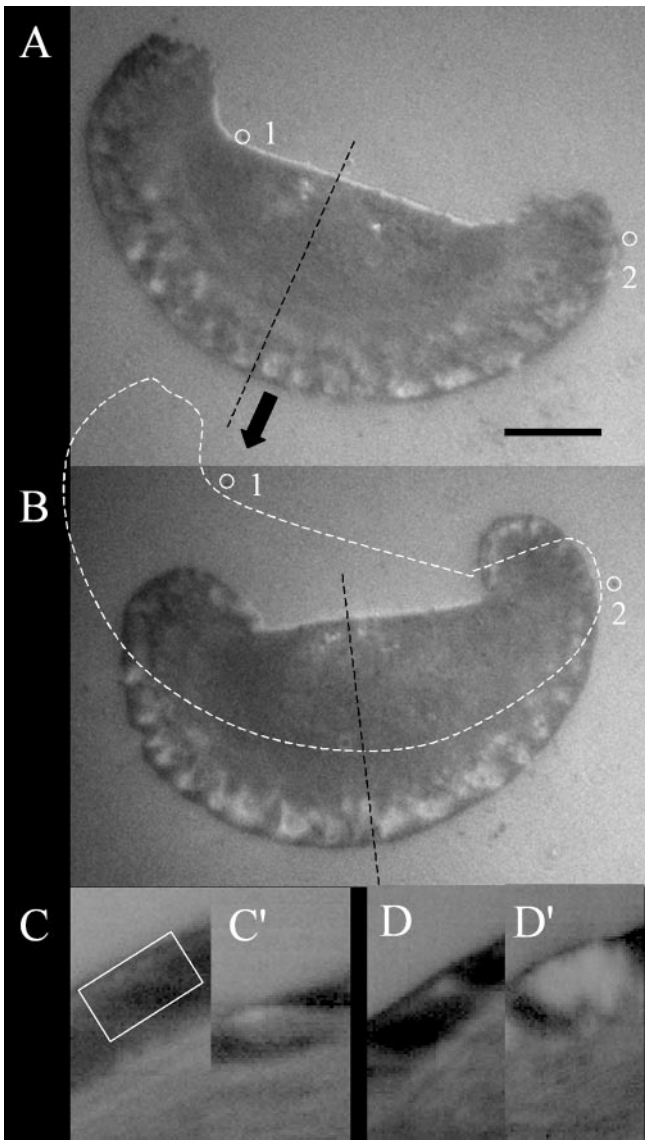

Figure 6. Interference reflection image of a keratocyte moving in the direction indicated (block arrow) before (A) and after (B) ML7 treatment. The cell outline of A is superimposed on B (dashed line) to indicate the distance traveled by the cell during the kymographs shown in C and C′. Marks that are stationary with respect to the substratum are indicated by numbered, open circles. Bar, 10 μm. Kymographs showing adhesion dynamics before (C and D) and after (C′ and D′) ML7 treatment. Kymograph (C) was obtained from the image slice shown in A (dashed black line) and C′ was obtained from B. Measurements of average brightness were taken from positions corresponding to the white open rectangle in C and were used as estimates of adhesiveness. Comparison of kymographs before and after treatment show that regions of close contact, at the leading edge, become lighter after ML7 treatment, suggesting a decrease in adhesiveness.

pare Figure 6, C with C′ and D with D′) consistent with a decrease in adhesiveness.

To investigate whether any change in distribution of adhesion molecules occurs, we immunostained 5-day-old keratocyte cultures for vinculin before and after treatment with ML7. In untreated cells, focal adhesions were clearly visible within the lamellae and along the outer cell margin in 86% of all cells examined (n = 30, Figure 7, A and B) These structures were found in only 30% of ML7 treated cells (n = 23) and were sparsely distributed adjacent to the cell body. In addition vinculin staining was often noticeably weaker than in untreated cells (Figure 7, C and D), and the lamellae were enlarged, consistent with an increase in protrusiveness.

The above findings provided a strong indication that ML7 decreases adhesiveness, so to test this possibility directly we performed shear flow experiments on single keratocytes before and after treatment with 10 μM ML7 (Figure 7E). We found that a shear force of ~300 dynes/cm^2 caused slight peeling of the lamella in 56% of untreated cells, whereas only 7% could be detached completely. The most obvious effect of ML7 treatment was to increase the number of cells sheared from the substratum to 43%. Another indication of a loss in adhesive strength was the increase in numbers of cells that underwent extensive lamellar peeling (20%), whereas fewer cells (33%) showed slight peeling of the cell edge, compared with untreated ones. In all experiments a range of responses to shear flow was observed, which reflects the heterogeneity in adhesion strength within any given population of keratocytes and which is suggested by the range of traction stress magnitudes that keratocytes can generate (Doyle and Lee, 2005). Together these data confirm that 10 μM ML7 leads to a significant decrease in cell adhesiveness.

DISCUSSION

We have investigated the relationship between the retrograde flow of actin, protrusion, and cell speed within the leading lamellipodium of fish keratocytes transfected with GFP-actin. Using FSM we have detected a retrograde flow of actin within the front of the lamellipodium, whose rate is inversely related to protrusion and cell speed. In addition we have examined the relationship between the retrograde flow of actin and traction force production in keratocytes using ML7, an inhibitor of MLCK, to reduce cytoskeletal contractility. Surprisingly, we found that ML7 treatment had opposite effects in fast- versus slow-moving cells, despite the fact that this treatment reduces contractility and adhesiveness in all cells. In fast-moving cells ML7 treatment increased retrograde flow rate but decreased protrusion and cell speed. Conversely, in slow-moving cells, the same treatment led to a decrease in retrograde flow but increased protrusion and cell speed. We conclude from this that there are two independent mechanisms for generating retrograde flow, which are associated with either decreased or increased traction force production.

Our detection of a retrograde flow of actin within front portions of the keratocyte lamellipodium was surprising in the light of previous work that showed the cytoskeleton to be stationary with respect to the substratum in this region (Theriot and Mitchison, 1991; Svitkina *et al.*, 1997; Verkhovsky *et al.*, 1999). The failure of previous work to detect retrograde flow at the front of keratocytes is most likely due to the fact that photoactivated or photobleached marks in the cytoskeleton remain clearly visible for only a short period of time (~30 s), so that slow (<3.5 μm/min) rates of retrograde flow would be undetectable. Nevertheless, evidence for a retrograde flow of actin was provided by the progressive curvature of photoactivated lines at the rear of keratocytes (Theriot and Mitchison, 1991) because this could only occur if the cytoskeleton was moving rearward with respect to both the substratum and the cell margin (Lee *et al.*, 1993). Therefore, the sensitivity of FSM and the relative

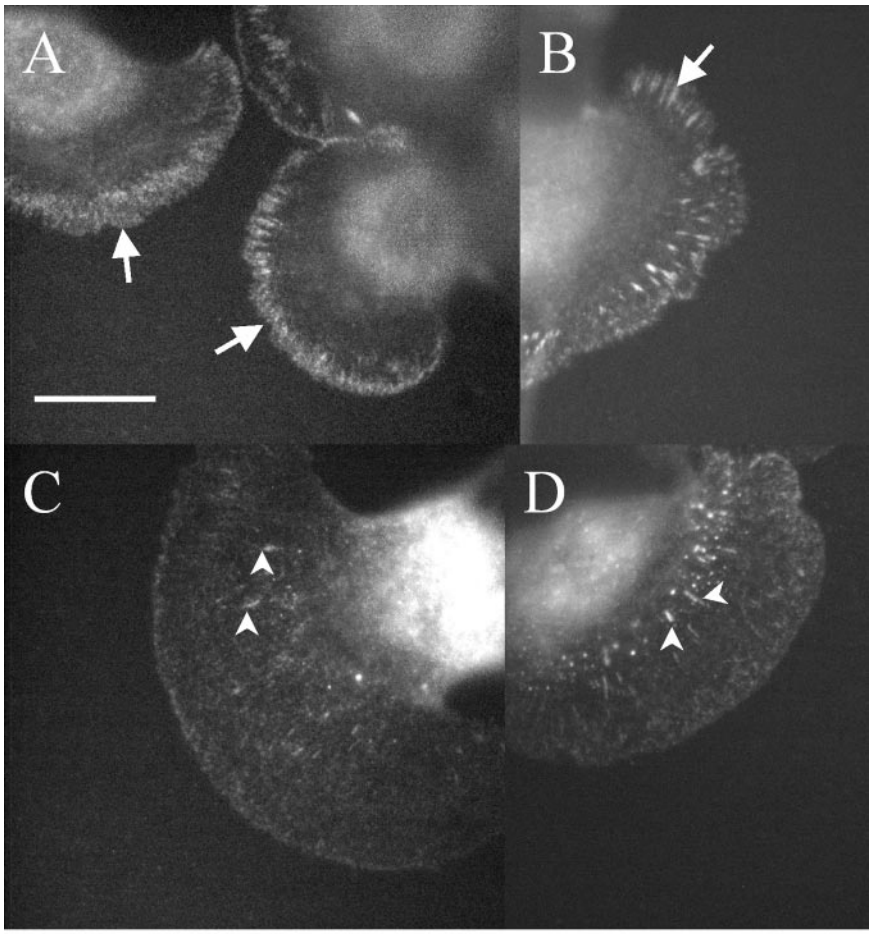

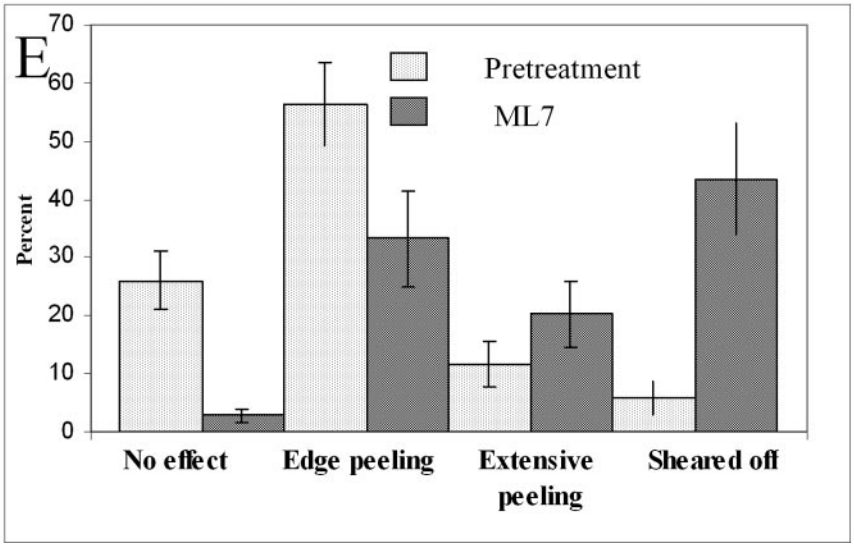

Figure 7. Immunofluorescence staining of vinculin in keratocytes before (A and B) and after (C and D) treatment with 10 μM ML7. Numerous punctae and small focal adhesions can be seen along the cell margin and within the lamellae of untreated cells (arrows). This is not seen in treated cells, except for a few sparsely distributed focal adhesions and punctae adjacent to the cell body (arrowheads). Bar, 10 μm. (E) Histogram showing the percentage and type of cellular response to shear flow, before and after ML7 treatment. These data were pooled from four separate experiments, n = 104, for all cells pretreatment and n = 152, or all cells post ML7 treatment. Error bars, SE of the mean.

simplicity of keratocyte movement have been of key importance for detecting small or subtle changes in retrograde flow at the leading edge.

The existence of a retrograde flow of actin within leading portions of the keratocyte lamellipodium, together with the recent detection of inward facing, propulsive, traction stresses in this region (Galbraith and Sheetz, 1999; Doyle *et al.*, 2004) is consistent with the "raking" hypothesis of traction force generation (Harris *et al.*, 1980; Harris, 1994). According to this idea, traction forces are generated when a contractile cytoskeleton that is mechanically coupled to adhesion receptors, rakes inward against the substratum. Alternatively, because traction forces at the leading edge are relatively small, it is possible that retrograde flow at the leading edge represents slippage between the cytoskeleton and substratum bound adhesion receptors, as described by the molecular clutch hypothesis (Lin and Forscher, 1994; Lin *et al.*, 1996). This is consistent with our finding that retro-

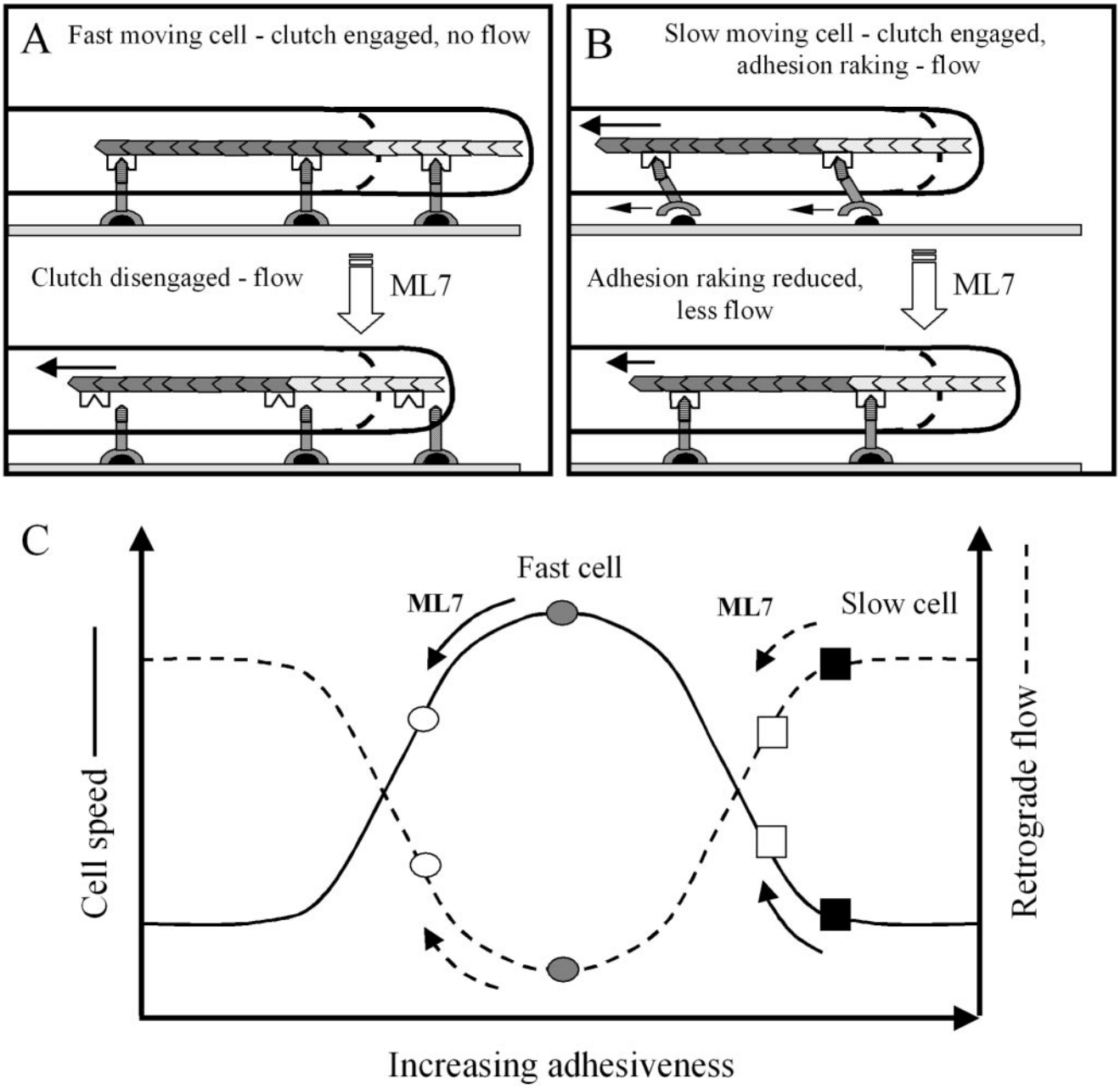

Figure 8. Diagrams of a protruding lamellipodium illustrating how retrograde actin flow can result from either (A) slippage between the cytoskeleton (stippled chevrons) and adhesion receptors (inverted Y-shaped symbols) or (B) raking between these receptors and their substratum bound ligands (black semicircles; B). ML7 treatment of fast-moving cells is proposed to disengage the molecular clutch (inverted M-shaped symbol) from the intracellular domain (horizontal striped region) of adhesion receptors. As a result retrograde flow increases and less newly polymerized actin (light stippled chevrons) can contribute to protrusion. (B) Raking between adhesion receptors (small, left pointing, arrows) and substratum bound ligands is shown occurring in a slow-moving cell, due to the generation of relatively large contractile forces (long arrow). In addition large contractile forces reduce the amount of actin polymerization that can contribute to protrusion. A ML7-induced reduction in contractility can reduce adhesion raking and associated retrograde flow, while increasing the rate of protrusion. (C) Hypothetical relationship between retrograde flow, cell speed and adhesiveness, that can account for the differential effects of ML7 on fast- and slow-moving cells. Cell speed (solid line) is shown to exhibit a biphasic relationship with respect to adhesiveness, which is also inversely related to retrograde flow. Rapid cell movement is shown (gray circle) to occur at an optimum level of adhesiveness, where retrograde flow is minimal. After ML7 treatment cell speed is reduced (○) and retrograde flow increases. Slow cell movement (■) is shown to occur when adhesiveness is above optimum levels and retrograde actin flow is high. After ML7 treatment adhesiveness is reduced closer to the optimum and retrograde flow is decreased (□).

grade flow is inversely proportional to both protrusion rate and cell speed. In addition, we found that retrograde flow rates (1–10 μm/min) in keratocytes are in the same range as those measured in *Aplysia* growth cones (Lin *et al.*, 1996) and sea urchin coelomocytes (Henson, 1999). There is also evidence that the molecular components of the molecular

clutch are the same in keratocytes as in other cell types. For example, β1-integrins and talin that form cytoskeletal-substratum linkages (Sydor *et al.*, 1996; Giannone *et al.*, 2003) are also found along the cell margin of keratocytes (Lee and Jacobson, 1997; Galbraith and Sheetz, 1999). Furthermore, engagement of the molecular clutch in keratocytes and other cell types appears to be regulated by mechanical stress. For instance, strengthening of adhesions and cytoskeletal-adhesion linkages occurs in response to force in both keratocytes (Lee and Jacobson, 1997; Galbraith and Sheetz, 1999), neuronal growth cones (Suter *et al.*, 1998), and fibroblasts (Choquet *et al.*, 1997; Riveline *et al.*, 2001).

Despite the evidence for the functioning of a molecular clutch in keratocytes, the increase in retrograde flow rate seen in fast-moving cells after ML7 treatment, contrasts with the reduction in retrograde flow observed in growth cones or coelomocytes, when myosin II is inhibited (Lin *et al.*, 1996; Henson *et al.*, 1999). Furthermore, a reduction in retrograde flow is normally associated with an increase in protrusion rate, not a decrease, as we observed in fast-moving keratocytes. Another puzzling aspect of our results is the differential response of fast- and slow-moving cells to ML7, particularly as a reduction in cytoskeletal contractility, occurs in all cells. So how can a reduction in contractility produce different effects in fast- and slow-moving cells and how can this be described in terms of the molecular clutch hypothesis? We propose that the answers to these questions lie in the biphasic relationship that exists between cell-substratum adhesiveness and cell speed (DiMilla *et al.*, 1991, 1993; Palecek *et al.*, 1997; Figure 8C) together with the inherent variation in adhesiveness between cells. It is generally accepted that cell movement is most rapid when adhesion strength is at an optimum level, such that it is strong enough to stabilize newly formed protrusions at the front, but sufficiently weak at the rear for retraction to occur. However, cell movement is inhibited if adhesiveness is above or below optimum adhesiveness. Our IRM, immunofluorescence, and shear flow data are in accord with a previous finding that ML7 treatment leads overall decrease in cell adhesiveness (Kaneko *et al.*, 2002). In fast-moving cells, whose adhesiveness was presumably close to optimal, decreases in both the rate of protrusion and cell speed suggest that adhesion strength is now suboptimal (Palecek *et al.*, 1997; Figure 8C). It is possible that ML7 leads indirectly to weakening of the cytoskeletal-adhesion linkages so that the cytoskeleton can now slip backward, even though cytoskeletal contractility is reduced (Palecek *et al.*, 1997; Figure 8A). Consistent with this is the finding that cytoskeletal-adhesion linkage strength is dependent on force (Choquet *et al.*, 1997; Suter and Forscher, 2001). In addition a reduction in cytoskeletal contractility has been shown to induce the disassembly of focal adhesions and reduce traction force production, as evidenced by the decreased wrinkling of a silicone rubber substratum (Leader *et al.*, 1983; Chrzanowska-Wodnicka and Burridge, 1996). The consequence of a slipping molecular clutch is that protrusion will be inhibited, because although adhesions are immobilized on the substratum, they cannot restrain the retrograde flow of actin, that could otherwise drive protrusion. The decrease in contractility will also inhibit retraction, resulting in an overall decrease in cell speed.

The increase in protrusiveness after ML7 treatment of initially slow-moving keratocytes, resembles the response of *Aplysia* growth cones to myosin II inhibition (Lin *et al.*, 1996). However, it is important to note that in our experiments, a decrease in traction force occurs that contrasts with the increased coupling between the cytoskeleton and adhesions seen in *Aplysia* growth cones (Suter *et al.*, 1998a, 1998b; Suter and Forscher, 2000). One explanation for this discrepancy is that before treatment, slow-moving cells were too adhesive and were generating large traction forces because of the raking of adhesion receptors against the substratum (Palecek *et al.*, 1997; Figure 8B). Direct evidence for raking is provided by observations that adhesions can slide rearward with respect to the substratum in stationary fibroblasts (Smilenov *et al.*, 1999) at the retracting cell margins moving keratocytes (Anderson and Cross, 2000) and motile sarcoma cells (Paku *et al.*, 2003). Raking could also explain why large traction forces are observed at the rear of keratocytes, where retrograde flow was sufficiently high to be detected by photoactivation experiments (Theriot and Mitchison, 1991; Lee *et al.*, 1993). Therefore, by reducing contractile forces, adhesion raking is reduced and protrusion can occur more efficiently. Another way to view this effect is that cell adhesiveness has moved closer to the optimum level (Palecek *et al.*, 1997; Figure 8C). This is consistent with the increase in cell speed that occurs and suggests that in addition to promoting protrusion, reduced contractility may also facilitate retraction. Although counterintuitive, a decrease in contractility could reduce clustering of adhesion components, and thus weaken adhesions sufficiently to allow retraction. Support for this idea comes from recent work showing that cytoskeletal contractility plays a role in clustering adhesion components (Delanoe-Ayari *et al.*, 2004).

We conclude that retrograde flow can result from either slippage of the molecular clutch or from adhesion raking. Although these two mechanisms may be indistinguishable from the appearance of retrograde grade flow, one major difference is that traction force production will be significantly lower when the clutch is slipping than when it is engaged and raking is occurring. Although we have discussed cytoskeleton-adhesion slippage and raking separately, it is likely that these two mechanisms are regulated concurrently. This may explain why in some instances an inverse relationship between retrograde flow and protrusion rate has not been observed (Theriot and Mitchison, 1992; Royal *et al.*, 1995). Despite these exceptions, the highly conserved nature of both the structural components and regulatory mechanisms of the molecular clutch mean that our findings in keratocytes will be highly relevant to a general mechanism of motility.

ACKNOWLEDGMENTS

We thank A. D. Doyle for the data contained in Figure 3, and N. N. Strickland for the immunofluorescence images in Figure 7. This work was supported by National Science Foundation grant MCB-0114231 to J.L.

REFERENCES

Anderson, K. I., and Cross, R.. (2000). Contact dynamics during keratocyte motility. Curr. Biol. *10*, 253–260.

Balaban, N. Q. *et al.* (2001). Force and focal adhesion assembly: a close relationship studied using elastic micropatterned substrates. Nat. Cell Biol. *3*, 466–472.

Beningo, K. A., Dembo, M., Kaverina, I., Small, V., and Wang, Y.-L. (2001). Nascent focal adhesions are responsible for the generation of strong propulsive forces in migrating fibroblasts. J. Cell Biol. *153*, 881–887.

Choquet, D., Felsenfeld, D. P., and Sheetz, M. P. (1997). Extracellular matrix rigidity causes strengthening of integrin-cytoskeleton linkages. Cell *88*, 39–48.

Chrzanowska-Wodnicka, M., and Burridge, K. (1996). Rho-stimulated contractility drives the formation of stress fibers and focal adhesions. J. Cell Biol. *133*, 1403–1415.

Cramer, L. P. (1997). Molecular mechanism of actin-dependent retrograde flow in lamellipodia of motile cells. Front. Biosci. *2*, d260–d270.

Davies, P. F., Robotewskyj, A., and Griem, M. L. (1993). Endothelial cell adhesion in real time. J. Clin. Invest. *91*, 2640–2652.

Davies, P. F., Robotewskyj, A., and Griem, M. L. (1994). Quantitative studies of endothelial cell adhesion. J. Clin. Invest. *93*, 2031–2038.

Delanoe-Ayari, H., Kurdi, R. A., Vallade, M., Gulino-Debrac, D., and Riveline, D. (2004). Membrane and acto-myosin tension promote clustering of adhesion proteins. Proc. Natl. Acad. Sci. USA *101*, 2229–2234.

Dembo, M., and Wang, Y.-L. (1999). Stresses at the cell-to-substrate interface during locomotion of fibroblasts. Biophys. J. *76*, 2307–2316.

DiMilla, P. A., Barbee, K., and Lauffenburger, D. A. (1991). Mathematical model for the effects of adhesion and mechanics on cell migration speed. Biophys. J. *60*, 15–37.

DiMilla, P. A., Stone, J. A., Quinn, J. A., Albelda, S. M., and Lauffenburger, D. A. (1993). Maximal migration of human smooth muscle cells on fibronectin and type IV collagen occurs at an intermediate attachment strength. J. Cell Biol. *122*, 729–737.

Doyle, A., and Lee, J. (2005). Cyclic changes in keratocyte speed and traction stress arise from Ca^{2+}-dependent regulation of cell adhesiveness. J. Cell Sci. (*in press*).

Doyle, A., Marganski, W., and Lee, J. (2004). Calcium transients induce spatially coordinated increases in traction force during the movement of fish keratocytes. J. Cell Sci. *117*, 2203–2214.

Doyle, A. D., and Lee, J. (2002). Simultaneous, real-time imaging of intracellular calcium and traction force production. Biotechniques *33*, 358–364.

Euteneuer, U., and Schliwa, M. (1984). Persistent, directional motility of cells and cytoplasmic fragments in the absence of microtubules. Nature *310*, 58–61.

Forscher, P., and Smith, S. J. (1988). Actions of cytochalasins on the organization of actin filaments and microtubules in a neuronal growth cone. J. Cell Biol. *107*, 1505–1516.

Fukui, Y., Kitanishi-Yumura, T., and Yumaura, S. (1999). Myosin-II independent F-actin flow contributes to cell locomotion in *Dictyostelium.* J. Cell Sci. *112*, 877–886.

Galbraith, C., and Sheetz, M. (1999). Keratocytes pull with similar forces on their dorsal and ventral surfaces. J. Cell Biol. *147*, 1313–1323.

Giannone, G., Jiang, G., Sutton, D. H., Critchley, D. R., and Sheetz, M. P. (2003). Talin1 is critical for force-dependent reinforcement of initial integrin-cytoskeleton bonds but not tyrosine kinase activation. J. Cell Biol. *163*, 409–419.

Grebecki, A. (1994). Membrane and cytoskeletal flow in motile cells with emphasis on the contribution of free-living amoeba. Int. Rev. Cytol. *148*, 37–79.

Harris, A. K. (1994). Locomotion of tissue culture cells considered in relation to ameboid locomotion. Int. Rev. Cytol. *150*, 35–68.

Harris, A. K., Wild, P., and Stopak, D. (1980). Silicone rubber substrata: a new wrinkle in the study of cell locomotion. Science *208*, 177–179.

Heideman, S., and Buxbaum, R. (1998). Cell crawling: first the motor, now the transmission. J. Cell Biol. *141*, 1–4.

Henson, J. H., Svitkina, T. M., Burns, A., Hughes, H. E., MacPartland, K. J., Nazarian, R., and Borisy, G. G. (1999). Two components of actin-based retrograde flow in sea urchin coelomocytes. Mol. Biol. Cell *10*, 4075–4090.

Horwitz, A. F., Duggan, K., Buck, C., Beckerle, M. C., and Burridge, K. (1986). Interactions of plasma membrane fibronectin receptor with talin—a transmembrane linkage. Nature *320*, 5312–5313.

Jay, D. G. (2000). The clutch hypothesis revisited: ascribing the roles of actin-associated proteins in filopodial protrusion in the nerve growth cone. Review. J. Neurobiol. *44*, 114–125.

Kaneko, K., Satoh, K., Masamune, A., Satoh, A., and Shomosegawa, T. (2002). Myosin light chain kinase inhibitors can block invasion and adhesion of human pancreatic cancer cell lines. Pancreas *24*, 34–41.

Leader, W. M., Stopak, D., and Harris, A. K. (1983). Increased contractile strength and tightened adhesions to the substratum result from reverse transformation of chinese hamster ovary cells by dibutyryl cyclic adenosine monophosphate. J. Cell Sci. *64*, 1–11.

Lee, J., Ishihara, A., Oxford, G., Johnson, B., and Jacobson, K. (1999). Regulation of cell movement is mediated by stretch-activated calcium channels. Nature *400*, 382–386.

Lee, J., Ishihara, A., Theriot, J., and Jacobson, K. (1993). Principles of locomotion for simple-shaped cells. Nature *362*, 167–171.

Lee, J., and Jacobson, K. (1997). The composition and dynamics of cell-substratum adhesions in locomoting fish keratocytes. J. Cell Sci. *110*, 2833–2844.

Lee, J., Leonard, M., Oliver, T., Ishihara, A., and Jacobson, K. (1994). Traction forces generated by locomoting keratocytes. J. Cell Biol. *127*, 1957–1964.

Lin, C. H., Espreafico, E. M., and Mooseker, M. S. (1996). Myosin drives retrograde F-actin flow in neuronal growth cones. Neuron *16*, 769–782.

Lin, C.-H., and Forscher, P. (1995). Growth cone advance is inversely proportional to retrograde F-actin flow. Neuron *14*, 763–771.

Lin, C.-H., Thompson, C. A., and Forscher, P. (1994). Cytoskeletal reorganization underlying growth cone motility. Curr. Opin. Neurobiol. *4*, 640–647.

Mallavarapu, A., and Mitchison, T. (1999). Regulating actin cytoskeleton assembly at filopodium tips controls their extension and retraction. J. Cell Biol. *146*, 1097–1106.

Marganski, W. A., Dembo, M., and Wang, Y.-L. (2003). Measurements of cell-generated deformations on flexible substrata using correlation-based optical flow. Methods Enzymol. *161*, 197–211.

Mitchison, T., and Kirschner, M. (1988). Cytoskeletal dynamics and nerve growth. Neuron *1*, 761–772.

Moazzam, F., DeLano, F. A., Zweifach, B. W., and Schmid-Schonbein, G. W. (1997). The leukocyte response to fluid shear stress. Proc. Natl. Acad. Sci. USA *94*, 5338–5343.

Munevar, S., Wang, Y.-L., and Dembo, M. (2001). Traction force microscopy in normal and H-ras transformed 3T3 fibroblasts. Biophys. J. *80*, 1744–1757.

Oliver, T., Dembo, M., and Jacobson, K. (1999). Separation of propulsive and adhesive traction stresses in locomoting keratocytes. J. Cell Biol. *145*, 589–604.

Paddock, S. W. (1989). Tandem scanning reflected light microscopy of cell-substratum adhesions and stress fibers in Swiss 3T3 cells. J. Cell Sci. *93*, 142–146.

Paku, S., Tovari, J., Lorincz, Z., Timar, F., Dome, B., Kopper, L., Raz, A., and Timar, J. (2003). Adhesion dynamics and cytoskeletal structure of gliding human fibrosarcoma cells: a hypothetical model of cell migration. Exp. Cell Res. *290*, 246–253.

Palecek, S. P., Loftus, J. C., Ginsberg, M. H., Lauffenberger, D. A., and Horwitz, A. F. (1997). Integrin-ligand binding properties govern cell migration speed through cell-substratum adhesiveness. Nature *385*, 537–540.

Riveline, D., Zamir, E., Balaban, N. Q., Schwarz, U. S., Ishizaki, T., Narumiya, S., Kam, Z., Geiger, B., and Bershadsky, A. (2001). Focal contacts as mechanosensors: externally applied local mechanical force induces growth of focal contacts by an mDia-dependent and ROCK-independent mechanism. J. Cell Biol. *153*, 1175–1185.

Roy, P., Petroll, W. M., Cavanagh, H. D., and Jester, J. V. (1999). Exertion of tractional force requires the coordinated up-regulation of cell contractility and adhesion. Cell Motil. Cytoskelet. *43*, 23–43.

Royal, D., Royal, M., Italiano, J., Roberts, T., and Soll, D. R. (1995). In *Ascaris* sperm pseudopods, MSP fibers move proximally at a constant rate regardless of the forward rate of cellular translocation. Cell Motil. Cytoskelet. *31*, 241–253.

Saitoh, M., Ishikawa, T., Matsushima, S., Naka, M., and Hidaka, H. (1987). Selective inhibition of catalytic activity of smooth muscle myosin light chain kinase. J. Biol. Chem. *262*, 7796–7801.

Smilenov, L. B., Mikhailov, A., Pelham, R. J., Marcantonio, E. E., and Gunderson, G. G. (1999). Focal adhesion motility revealed in stationary fibroblasts. Science *286*, 1172–1174.

Suter, D., and Forscher, P. (2001). Transmission of growth cone traction force through apCAM-cytoskeletal linkages is regulated by Src family tyrosine kinase activity. J. Cell Biol. *155*, 427–438.

Suter, D. M., Errante, L. D., Belotserkovsky, V., and Forscher, P. (1998). The immunoglobulin superfamily cell adhesion molecule, apCAM, mediates growth cone steering by substrate-cytoskeletal coupling. J. Cell Biol. *141*, 227–240.

Suter, D. M., and Forscher, P. (1998). An emerging link between cytoskeletal dynamics and cell adhesion molecules in growth cone guidance. Curr. Opin. Neurobiol. *8*, 106–116.

Suter, D. M., and Forscher, P. (2000). Substrate-cytoskeletal coupling as a mechanism for the regulation of growth cone motility and guidance. J. Neurobiol. *44*, 97–113.

Svitkina, T. M., Verkhovsky, A. B., Quade, K.M.M., and Borisy, G. C. (1997). Analysis of the actin-myosin II system in fish epidermal keratocytes: mechanism of cell body translocation. J. Cell Biol. *139*, 397–415.

Sydor, A. M., Su, A. L., Wang, F. S., Xu, A., and Jay, D. G. (1996). Talin and vinculin play dintinct roles in filopodial motility in neuronal growth cones. J. Cell Biol. *134*, 1197–1208.

Theriot, J. A., and Mitchison, T. J. (1991). Actin microfilament dynamcs in locomoting cells. Nature *352*, 126–131.

Theriot, J. A., and Mitchison, T. J. (1992). Comparison of actin and cell surface dynamics in motile fibroblasts. J. Cell Biol. *118*, 367–377.

Verkhovsky, A. B., Svitkina, T. M., and Borisy, G. G. (1999). Self-polarization and directional motility of cytoplasm. Curr. Biol. *9*, 11–20.

Wang, Y.-L. (1985). Exchange of actin subunits at the leading edge of living fibroblasts: possible role of treadmilling. J. Cell Biol. *101*, 597–602.

Watanabe, N., and Mitchison, T. J. (2002). Single-molecule speckle analysis of actin filament turnover in lamellipodia. Science *295*, 1083–1086.

Waterman-Storer, C. M., Desai, A., Bulinski, J. C., and Salmon, E. D. (1998). Fluorescent speckle microscopy, a method to visualize the dynamics of protein assemblies in living cells. Curr. Biol. *8*, 1227–1230.